AIAA JOURNAL
Vol. 34, No. 9, September 1996

Micromechanics of Composites with Shape Memory Alloy Fibers in Uniform Thermal Fields

Victor Birman*
University of Missouri–Rolla, St. Louis, Missouri 63121
Dimitris A. Saravanos†
Ohio Aerospace Institute, Cleveland, Ohio 44142
and
Dale A. Hopkins‡
NASA Lewis Research Center, Cleveland, Ohio 44135

Analytical procedures are developed for a composite system consisting of shape memory alloy fibers within an elastic matrix subject to uniform temperature. A three-phase concentric cylinder model is developed for the analysis of local stresses, which includes the fiber, the matrix, and the surrounding homogenized composite. The solution addresses the complexities induced by the nonlinear dependence of the in situ martensite fraction of the fibers on the local stresses and temperature and the local stresses developed from interactions between the fibers and matrix during the martensitic and reverse phase transformations. Results are presented for a Ni-44.8wt% Ti/epoxy composite. The applications illustrate the response of the composite in isothermal longitudinal loading and unloading. The local stresses developed in the composite under various stages of the martensitic and reverse phase transformations are also shown.

Introduction

SHAPE memory alloys (SMAs) have found increasing applications as candidate smart materials and components of adaptive structures.[1] One potential application of shape memory alloys is their use as fibrous sensors or actuators within a composite material system. The development of such fibrous shape memory (SM) composites will provide weight savings, directionality in actuation and sensing, and some control over the resultant SM effect. Some technical details of such applications were discussed by Schetky and Wu,[2] Schetky,[3] and White et al.[4] The use of shape memory alloys as sensors may be related to the dependence of their properties on the martensite fraction (for example, their electric resistance).[5] Conversely, the use of SMA fibers as distributed micro-actuators is also very attractive because of the relatively high strains that can be generated.

In summary, the SM effect is associated with a martensitic phase transformation of the material from a parent phase.[1] During such martensitic transformations, changes in crystallography result in substantial strains, called transformation strains. Of particular interest are alloys that can recover their parent phase through a reverse phase transformation accompanied by recovery strains. These are SMAs that can undergo thermoelastic or complete phase transformations. In addition to the transformation strains, the phase transformations are accompanied by changes in the elastic, thermal, and electric properties. The initiation of the martensitic or the reverse transformation depends on the free chemical energy in the material, which, in turn, depends on the temperature and stress state. Hence, in a SM composite, the actuation process may be achieved by forcing the phase transformation to occur in the fibers by changing either the temperature or the stresses[3] in the fibers.

Constitutive relations required to characterize the thermomechanical response of SMAs were outlined in the works of Baumgart et al.,[6] Tanaka,[7] Sato and Tanaka,[8] and Brinson.[9] Applications of the unidirectional shape memory effect can be found in Refs. 10–14. Liang and Rogers[15] and Boyd and Lagoudas[16] have provided formulations for the three-dimensional SM effect.

The analysis of composites incorporating continuous SMA fibers seems a rather open-ended research area involving solution of several problems including admissible micromechanics and the nonlinear constitutive relations of SMAs. Indeed, the properties and the induced strain of the SMA fibers depend on the fraction of martensite, which, in turn, depends on the in situ temperature and effective stress state. Because of the fiber–matrix interaction in the composite, the developed in situ stresses will depend on phase transformation strains, thermal strains, and the constituent properties. This interdependence results in a nonlinear thermomechanical response (even by assuming thermoelastic austenite and martensite phases), which makes an iterative analysis seemingly necessary, although, as shown in the present paper, an analytical solution may be obtained in some cases without iterations. Numerous micromechanical theories may be used to formulate the present problem, yet limited work has been reported in the area of SM composites. Three-dimensional micromechanics were reported by Boyd and Lagoudas[16] using the micromechanics approach of Mori and Tanaka[17] and by Sulivan and Buesking[18] using primarily Hashin's[19] vanishing fiber concentric cylinder assemblage method. The previous micromechanics are valid approaches that may yield good approximations of the equivalent properties of composites[20]; however, the assumptions of average constituent stresses/strains may be an area of limitation, as they may not yield the variation of stresses in the various constituents of the composite.

The present paper presents a combined micromechanical approach that has the potential to provide better representations of local stresses in an SM composite. A three-phase concentric cylinder model (SMA fiber, matrix, equivalent SM composite) is formulated. The third infinite cylinder of equivalent SM composite has been introduced to account for the interactions with the surrounding fibers/matrix. The properties of the composite medium enclosing the SMA fibers are calculated by extending the multicell micromechanics approach of Chamis.[21] An analytical solution is obtained,

Presented as Paper 95-1210 at the AIAA/ASME/AHS/ASC 36th Structures, Structural Dynamics, and Materials Conference, New Orleans, LA, April 10–13, 1995; received June 9, 1995; revision received April 15, 1996; accepted for publication May 19, 1996.

*Professor, Engineering Education Center, 8001 Natural Bridge Road.
†Senior Research Associate, 22800 Cedar Point Road. Member AIAA.
‡Acting Branch Chief, Structural Mechanics Branch, MS 23-3. Member AIAA.

which yields the response of the SM composite in longitudinal loading and the corresponding fields of local stresses (microstresses). Results quantify the isothermal loading-unloading response of the composite under various temperature and initial stress conditions, the capability of the composite to undergo temperature-induced actuation, and the resultant local stresses in the composite during a loading-unloading cycle with stress-induced phase transformation in the fibers.

Constitutive Equations

The assumed constitutive equations of the SMA fibers, the matrix, and the resultant SM composite are presented in this section. The fibers and the matrix are assumed to remain within the linear elastic range, which is a reasonable assumption since plasticity seems to usually occur after the martensitic transformation. Both the fibers and matrix are assumed isotropic. However, the composite is transversely isotropic with a plane of symmetry transversely to the fibers.

Fibers

Assuming that both martensitic and parent phases are isotropic and that there is no directionality in the alignment of the martensite and austenite crystals, the SMA fibers may be assumed to remain isotropic, and their engineering properties are linear functions of the martensite fraction (rule of mixtures)[14-16]

$$\{P_f\} = \xi\{P_f^M\} + (1-\xi)\{P_f^A\} \tag{1}$$

where P represents the thermoelastic properties, subscript f indicates the fiber, ξ is the current martensite volume fraction in the fiber, and superscripts M and A identify the martensite and austenite (parent) phases, respectively.

Considering that the austenite and martensite phases in an SMA are assumed to behave thermoelastically, the behavior of an SMA fiber during the martensite or reverse phase transformation may be effectively described by Hooke's law in expanded form,[16]

$$\sigma_{fi} = C_{fij}(\epsilon_{fj} - \alpha_{fj}\Delta T - \epsilon_j^t), \qquad i, j = 1, \ldots, 6 \tag{2}$$

where σ_{fi} is the stress vector, ϵ_j is the elastic strain vector, ΔT is the temperature variation, and C_{ij} and α_j are the current elasticity tensor and the vector of thermal expansion coefficients, respectively. The term ϵ_j^t is the transformation strain as a result of phase change. There is reasonably good understanding and experimental evidence about the uniaxial behavior of SM materials; that is, under uniaxial stress the rate of the transformation strain is directly proportional to the rate of the martensite fraction,

$$\dot{\epsilon}^t = \omega\dot{\xi} \tag{3}$$

where ω is the maximum transformation state in uniaxial isothermal loading. However, the behavior of SMAs under a three-dimensional stress state seems to be less understood, particularly the effect that individual stress components may have on the reorientation of the martensite variants. The relationship between the transformation strain and martensite fraction may have the general form[15,16,22]

$$\dot{\epsilon}_i^t = \Lambda_i\dot{\xi}, \qquad i = 1, \ldots, 6 \tag{4}$$

Liang and Rogers[15] and Boyd and Lagoudas[16,22] have proposed various forms for the transformation tensor Λ_i, which effectively assume that the transformation strain is also related to the deviatoric stress components. Although these are interesting approaches attempting to capture the interactions between the various stress components and the corresponding transformation strain, the proposed forms of Λ_i and underlying assumptions have been neither validated nor correlated with experimental data. In the present paper, the transformation tensor components were assumed proportional to the maximum transformation strain ω_i being observed when the corresponding uniaxial stress component was applied; i.e., $\Lambda_i = \omega_i$. Then the integration of Eq. (4) results in

$$\epsilon_i^t - \epsilon_i^{0t} = \omega_i(\xi - \xi^0), \qquad i = 1, \ldots, 6 \tag{5}$$

where superscript 0 refers to an initial state. Equation (2) can be applied at different time instances (as in the case of uniaxial phase transformation[10,14]) to yield

$$\sigma_{fi} - \sigma_{fi}^0 = C_{fij}(\xi)\{\epsilon_{fj} - \alpha_{fj}(\xi)\Delta T - \omega_{fj}\xi\} - C_{fij}(\xi^0)\{\epsilon_{fj}^0 - \alpha_{fj}(\xi^0)\Delta T^0 - \omega_{fj}\xi^0\} \tag{6}$$

In thermoelastic martensitic transformations, the martensite fraction depends on the free chemical energy in the material, which, in turn, includes the thermal and strain energy components. This relation may be represented by phenomenological equations[7,8] that use the effective stress to represent the three-dimensional stress state in the material.[15,16] Accordingly, during the martensite transformation,

$$\xi = 1 - \exp\left[b_M(T_S^M - T) + c_M\sigma_{\text{eff}}\right] \tag{7}$$

and during the reverse transformation,

$$\xi = \exp\left[b_A(T_S^A - T) + c_A\sigma_{\text{eff}}\right] \tag{8}$$

where T_S^M and T_S^A are the martensite and austenite phase start temperatures under reference stress-free conditions and σ_{eff} is the effective stress defined as

$$\sigma_{\text{eff}} = \left(\tfrac{3}{2}\sigma_{ij}'\sigma_{ij}'\right)^{\frac{1}{2}}, \qquad \sigma_{ij}' = \sigma_{ij} - \tfrac{1}{3}\sigma_{kk}\delta_{ij}, \qquad i, j, k = 1, \ldots, 3 \tag{9}$$

The coefficients b_M, c_M, b_A, and c_A are given by

$$b_M = \frac{\ell n 0.01}{T_S^M - T_F^M} \qquad c_M = \frac{b_M}{d_M}$$
$$b_A = \frac{\ell n 0.01}{T_S^A - T_F^A} \qquad c_A = \frac{b_A}{d_A} \tag{10}$$

where T_F^M and T_F^A are the martensite and austenite finish temperatures under stress-free conditions and d_M and d_A are constants defining the slopes of the martensitic and reverse transformation lines on the stress–temperature diagram, respectively. The characteristic temperatures depend also on the effective stress:

$$\langle \bar{T}_S^M, \bar{T}_F^M \rangle = \langle T_S^M, T_F^M \rangle + (\sigma_{\text{eff}}/d_M)$$
$$\langle \bar{T}_S^A, \bar{T}_F^A \rangle = \langle T_S^A, T_F^A \rangle + (\sigma_{\text{eff}}/d_A) \tag{11}$$

where the overbar indicates the start and finish temperatures of the respective phase transformation in the presence of stress. Equations (7) and (8) may be rearranged to provide the range of the effective stress where stress-induced martensitic and reverse phase transformations (at a prescribed temperature) will occur, respectively:

$$\frac{b_M}{c_M}(T - T_s^M) \le \sigma_{\text{eff}} \le \frac{\ell n 0.01}{c_M} + \frac{b_M}{c_M}(T - T_s^M) \tag{12}$$

$$\frac{\ell n 0.01}{c_A} + \frac{b_A}{c_A}(T - T_s^A) \le \sigma_{\text{eff}} \le \frac{b_A}{c_A}(T - T_s^A) \tag{13}$$

Equations (12) and (13) are obtained in accordance with the metallurgical approach, by identifying the values $\xi = 0.99$ and 0.01 with the completion of the martensite and reverse transformations, respectively.

Matrix

The matrix is assumed to be isotropic and elastic, such that

$$\sigma_{mi} = C_{mij}(\epsilon_{mj} - \alpha_{mj}\Delta T), \qquad i, j = 1, \ldots, 6 \tag{14}$$

where ΔT is the difference between the current and stress-free temperatures and subscript m indicates the matrix.

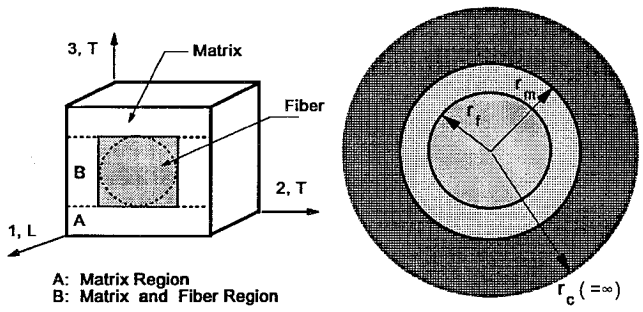

a) Multicell model b) Concentric cylinders model

Fig. 1 Representative composite models.

Composite

The equivalent constitutive equations for a composite medium with SMA fibers undergoing a martensitic or reverse transformation can be postulated to have the following form:

$$\sigma_{ci} = C_{cij}(\xi)\{\epsilon_{cj} - \alpha_{cj}(\xi)\Delta T - \omega_{cj}\xi\}, \qquad i, j = 1, \ldots, 6 \tag{15}$$

where subscript c indicates the homogenized composite and ξ is the martensite phase fraction in the fibers. The main difference with Eq. (2) is that the resultant composite will exhibit orthotropy in the LT plane (see Fig. 1), including the components of the maximum transformation strains. Equations (2), (6), and (15) remain valid during the martensitic and reverse transformation, and they reflect the behavior of thermoelastic SMA materials stressed below their second yield limit associated with the plastic slip of the martensitic phase.[23] In all cases, the initial conditions corresponding to the particular phase of the transformation should be considered; moreover, the continuity of stress–strain curves at the boundaries of adjacent transformation phases is preserved. It is finally emphasized that although Eqs. (6) and (15) can describe both martensitic and reverse transformations, the corresponding stress–strain curves do not overlap each other, because of the differences between the effective start and finish stresses and temperatures defining the onset and completion of the martensite and reverse phase transformations [see Eqs. (7) and (8) or (12) and (13)].

Micromechanics

Two different micromechanical approaches are presented. A concentric three-phase cylinder model is the primary micromechanics approach that is used to predict the response of an SM composite and the corresponding microstresses. However, a priori knowledge of the equivalent properties of the SM composite phase is required in the proposed concentric cylinder model. These equivalent properties of the SM composite were calculated by extending the multicell micromechanics method.[21,24,25]

Multicell Approach

Good approximations of the equivalent properties of the SM composite may be obtained using the multicell micromechanics approach.[21,24,25] According to the method, the representative cell is divided into a set of subregions (see Fig. 1a), each one containing portions of a square SMA fiber and the matrix. It is further assumed that the strains/stresses in the various subregions of the representative cell are uniform, the Poisson's effect on transverse deformations is negligible, and the fibers are packed in a square array formation. The analysis employs a mechanics of materials approach based on the equilibrium of stresses within each subregion and the compatibility of strains at the boundaries of each subregion. Thus, the equivalent constitutive relations of the SMA composite are derived in accordance with Eq. (15). The resultant expressions for the elastic and thermal properties are similar to the ones reported for thermoelastic composites and are shown in the Appendix. According to the constitutive relations for the fibers (2) and the composite (15), the phase transformation/recovery strain component has an analogous form to the thermal strain component. Therefore, at a given temperature and martensite fraction in the fibers, the equivalent maximum transformation strains of the composite ω_{ci} may be evaluated similarly to the thermal expansion coefficient of the composite (see the Appendix):

$$\omega_{c1} = \omega_{cL} = k_f \omega_f (E_f/E_L)$$

$$\omega_{c2} = \omega_{c3} = \omega_{cT} = \frac{k_f \omega_f}{1 - \sqrt{k_f}[1 - (E_m/E_f)]} \frac{E_m}{E_T} \tag{16}$$

where subscripts L and T indicate the longitudinal and transverse direction in the composite with respect to the fibers, k_f is the fiber volume fraction, E_f and E_m are the moduli of elasticity of the fiber and matrix, respectively, and E_L and E_T are the longitudinal and transverse moduli of elasticity of the composite medium.

Concentric Cylinder Approach

Considering the potential significance of local stresses (microstresses) in the response of the SMA fibers, a concentric cylinder model can provide better representations of the local stresses, which may have an effect on the axial response of the SMA composite. The three-cylinder assembly model shown in Fig. 1b was formulated containing a fiber, surrounded by a matrix and an infinite SM composite medium. The constitutive relations of the composite phase are provided by Eq. (15), and equivalent properties are provided by the previously described multicell micromechanics. The inclusion of the infinite composite cylinder is important, because it introduces the interactions of the fiber and matrix with the surrounding fibers as a result of the mismatch in the respective elastic, thermal, and transformation strains. Thus, the consideration of a surrounding infinite composite instead of a surrounding infinite matrix extends the application of the approach beyond the low fiber volume ratio regime.

Considering the axisymmetry of the problem, and assuming that the displacement u in the direction of the fiber remains uniform in the transverse r–θ plane, the nonzero strains are

$$\epsilon_\theta = \frac{w}{r}, \qquad \epsilon_r = \frac{\mathrm{d}w}{\mathrm{d}r}, \qquad \epsilon_x = \text{const} \tag{17}$$

where w is the displacement in the radial direction. The equations of equilibrium within each material region of the concentric cylinder model (fiber, matrix, and composite) are reduced to the following one:

$$\frac{\mathrm{d}\sigma_r}{\mathrm{d}r} + \frac{\sigma_r - \sigma_\theta}{r} = 0 \tag{18}$$

where subscripts x, r, and θ indicate longitudinal, radial, and tangential directions, respectively. Combination of Eq. (18) with constitutive equations results, in each region, in the following:

$$\frac{\sigma_r - \sigma_\theta}{r} = (C_{\theta\theta} - C_{\theta r})\frac{1}{r}[\epsilon_r - \epsilon_\theta - (\alpha_r - \alpha_\theta)\Delta T - (\omega_r - \omega_\theta)\xi]$$

$$\sigma_{r,r} = C_{r\theta}\epsilon_{\theta,r} + C_{rr}\epsilon_{r,r} - (C_{r\theta}\alpha_\theta + C_{rr}\alpha_r)\Delta T_{,r}$$

$$- (C_{r\theta}\omega_\theta + C_{rr}\omega_r)\xi_{,r} \tag{19}$$

Considering the transverse isotropy of each phase (fibers, matrix, and composite), the uniform temperature ($\Delta T_{,r} = 0$), and combining Eqs. (17–19), the following equation results:

$$C_{rr}(r^2 w_{,rr} + r w_{,r} - w) - (C_{rr} - C_{r\theta})r(\omega_r - \omega_\theta)\xi$$

$$- (C_{r\theta}\omega_\theta + C_{rr}\omega_r)r^2\xi_{,r} = 0 \tag{20}$$

The preceding equation is further simplified by considering the transverse isotropy of the transformation tensor and by assuming constant martensite fraction in the fiber ($\xi_{,r} = 0$). Under these assumptions, the admissible solution of Eq. (20) will have the form

$$\begin{Bmatrix} w_f \\ w_m \\ w_c \end{Bmatrix} = \begin{Bmatrix} A_1^f \\ A_1^m \\ A_1^c \end{Bmatrix} r + \begin{Bmatrix} A_2^f \\ A_2^m \\ A_2^c \end{Bmatrix} r^{-1} \tag{21}$$

where A_k^j are constants of integration and superscripts indicate the constituent. The requirements of a bounded solution yield $A_1^c = A_2^f = 0$. The remaining constants of integration are related via the conditions of continuity in the displacements and stresses at the fiber–matrix and matrix–composite interfaces:

$$\begin{aligned} w^f(r_f) &= w^m(r_f) \qquad \sigma_r^f(r_f) = \sigma_r^m(r_f) \\ w^m(r_m) &= w^c(r_m) \qquad \sigma_r^m(r_m) = \sigma_r^c(r_m) \end{aligned} \tag{22}$$

where r_f and r_m are the radius of the fiber and the external matrix interface (Fig. 1b), respectively.

The effective stress in the fibers [Eq. (9)], required for the determination of the martensitic fraction [Eqs. (7) and (8)] and the state of the composite, becomes

$$\sigma_{\text{eff}} = \left(\tfrac{3}{2}\sigma'_{ij}\sigma'_{ij}\right)^{\frac{1}{2}}$$

$$= \left\{\tfrac{1}{2}\left[\left(\sigma_x^f - \sigma_\theta^f\right)^2 + \left(\sigma_x^f - \sigma_r^f\right)^2 + \left(\sigma_r^f - \sigma_\theta^f\right)^2\right]\right\}^{\frac{1}{2}} \tag{23}$$

because the shear stresses are zero. The solution yields equal tangential and radial strains in the fiber, that is, $\epsilon_\theta = \epsilon_r = A_1^f$. Considering the isotropy in the transverse plane of the fiber, this also implies that the radial and tangential stresses in the fiber are equal and remain constant along the radial direction. This simplifies further the expression for the effective stress in the fibers:

$$(\sigma_{\text{eff}})_f = \left|\sigma_x^f - \sigma_r^f\right|_f \tag{24}$$

Computational Procedure

As seen in the previous analytical formulation, the analysis of both the properties and the local stresses in a fibrous SM composite may require an incremental and iterative approach. This is because the properties of the fibers and, therefore, the average properties of the composite depend on the stresses via the martensite fraction. In turn, the stresses are affected by the properties of the constituent materials. To further complicate the problem, the start and finish temperatures of the martensitic and reverse transformation depend also on the stresses.

However, the iterative process can be avoided, and the solution may be obtained directly. In the latter approach, the analysis begins by specifying the value of the temperature. Rather than specifying the axial strain or stress, the effective stress in the fiber is specified. Then the martensite fraction in the fiber is calculated according to Eq. (4) or (5). Once the martensitic function is defined, the properties of the fibers and the equivalent properties of the surrounding composite are calculated. Then, Eqs. (22) and (24) are solved, and the constants of integration A_1^f, A_1^m, A_2^m, and A_2^c and the axial strain ϵ_x corresponding to the effective stress are found. The local strains and stresses are calculated. A final integration over the radius yields the average longitudinal stress in the composite,

$$\sigma_{cx} = \frac{1}{r_m^2}\int_0^{r_m} \sigma_x r \, dr \tag{25}$$

Application Cases

The application cases presented in the following paragraphs illustrate the predicted stress–strain response of the composite under isothermal loading and unloading conditions, the capability of the composite to induce axial strains as a result of variations in the temperature, and the developed local stress fields in the material during stress-induced martensitic and reverse transformations in the fiber. The shape memory material considered in the examples is Ni-44.8wt% Ti, whose properties are presented in Table 1 as reported by Lei and Wu.[26] An epoxy matrix was assumed with properties shown in Table 1, and the fiber volume fraction was taken equal to 0.3.

Composite Response

The predicted loading and unloading cycle of the SM composite at 40°C is shown in Fig. 2. It was assumed that local nonmechanical stresses (stresses arising from mismatch in the transformation strains and the thermal strains between the fiber and the matrix)

Table 1 Properties of Ni-44.8wt% Ti fibers[26] (annealing temperature 600°C)

Property	Ni-44.8wt% Ti	Epoxy
E^A, GPa	30.0	3.4475
E^M, GPa	13.0	—
ν	0.33	0.35
α^A, 10^{-6}/°C	12.5	64.8
α^M, 10^{-6}/°C	18.5	—
T_s^M, °C	23	—
T_f^M, °C	5	—
T_s^A, °C	29	—
T_f^A, °C	51	—
d_M, MPa/°C	11.3	—
d_A, MPa/°C	4.5	—
$\omega_1 = \omega_2 = \omega_3 =$	0.07	—
$\omega_4 = \omega_5 = \omega_6 =$	0	—

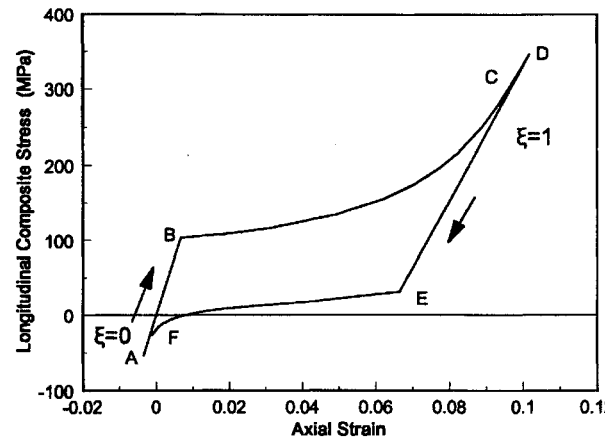

Fig. 2 Isothermal stress–strain cycle of 30% fiber volume ratio Ni-44.8wt% Ti/epoxy composite (40°C). Stress-free conditions correspond to austenite fibers.

are zero when the fibers are in the austenite phase. Practically, this implies that the SM composite was fabricated and matrix consolidation occurred at 40°C with the fibers in the austenite phase. As seen in Fig. 2, the composite deforms linearly from point A to B because the fibers remain in the austenite phase ($\xi = 0$). After point C the effective stress in the fiber becomes sufficiently high for the martensite transformation to start. The tensile transformation strain in the fibers results also in elongation of the composite. As a result of the transformation strain, local (compressive) longitudinal and radial stresses are also developed in the fiber, which start contributing to the effective stress [Eq. (24)], thus resulting in the nonlinear segment BC ($0 < \xi < 1$). At point C the fibers are fully transformed to the martensite phase ($\xi = 1$), and the subsequent linear section CD illustrates the behavior of the composite with elastic martensite fibers. The different slopes of sections AB and CD represent the differences in the moduli of the martensite and austenite phases of the fiber. The predicted unloading phase is also shown in section DEF. As the stress is reduced, the fibers remain in the martensitic phase until the reverse transformation starts (point E). Further stress reductions after point E reduce the martensite fraction in the fibers and the recovery strains, resulting in the nonlinear curve EF ($1 > \xi > 0$). After point F the fibers are fully transformed to their parent phase ($\xi = 0$) and the subsequent unloading follows the linear path FA.

The isothermal unloading of the previous SM composite system (reverse transformation of the SMA fibers) at four different temperatures is shown in Fig. 3. As in the previous case, the composite is free of local stresses when the fibers are austenite at 40°C. As seen in Fig. 3, at higher temperatures higher longitudinal stresses are required for starting and finishing the reverse transformation in the fibers. Figure 3 implicitly illustrates the potential of SM composites to be used as strain or stress actuators by varying the temperature of the composite, as well as quantifies the ranges of stress, strain, and temperature where such actuation is feasible. Within this range,

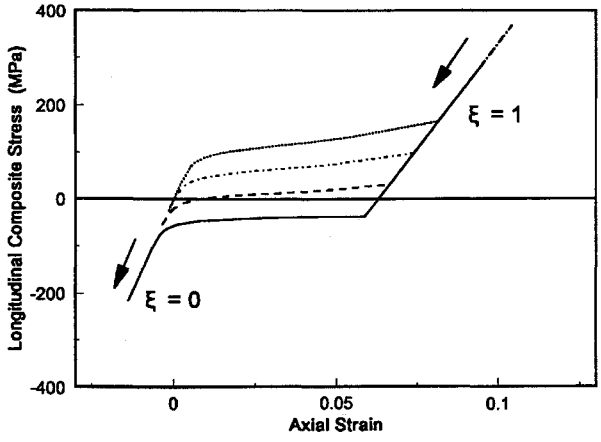

Fig. 3 Isothermal unloading of 30% fiber volume ratio Ni-44.8wt% Ti/epoxy composite at various temperatures. Stress-free conditions correspond to austenite fibers: ——, 20°C; – – –, 40°C; ·····, 60°C; and ····, 80°C.

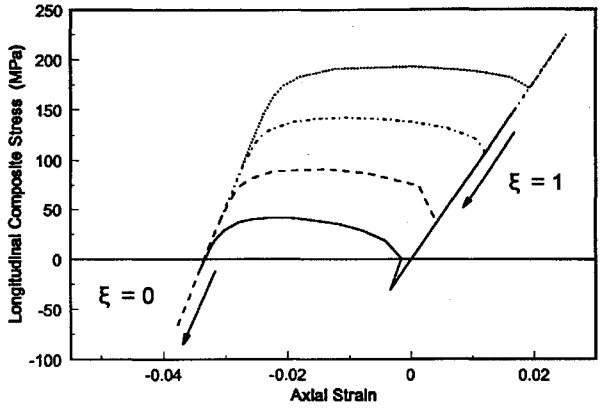

Fig. 4 Isothermal unloading of 30% fiber volume ratio Ni-44.8wt% Ti/epoxy composite at various temperatures. Stress-free conditions correspond to martensite fibers: ——, 20°C; – – –, 40°C; ·····, 60°C; and ····, 80°C.

the composite has the potential to generate significant longitudinal deformations or stresses. In all cases shown in Fig. 3, high recovery strains on an order of 6–8% have been calculated. Outside this range of stresses, the SM composite cannot act as an actuator. However, as shown in the following case, it seems that this range may be modified by changing the processing conditions.

Figure 4 also shows the isothermal unloading of the SM composite; however, in this case fabrication and matrix consolidation were assumed to take place when the fibers are in the martensitic phase at 40°C (thermal residual stresses are zero at 40°C). By fabricating the composite with the fibers in martensite phase, different initial states of local stresses are developed in the composite compared with the previous case, which result in the drastically different unloading behavior of Fig. 4. The reverse transformation occurs at different stress and strain ranges, and the recovery strains are smaller, on an order of 4% or less. This illustrates that the range of actuation of SM composites may be modified by controlling the initial local stresses in the composite. The predicted nonlinear unloading curve is also nonmonotonic with respect to the stress. To qualitatively explain this behavior, consider the stress–strain curve at 40°C, because the composite is free from thermal residual stresses at this temperature. First note that a tensile stress should be applied on the composite to have martensite fibers, which correctly reflects the need to have prestressed fibers, before and after the fabrication of the composite, for the martensite phase to exist at 40°C ($T > T_s^M$). As the axial strain is reducing, the effective stress in the fibers becomes sufficiently small to initiate the reverse transformation. The onset of reverse transformation in the fibers and the associated contractive transformation strains result in substantial monotonic contraction of the composite. However, a strain mismatch is also initiated between the fibers and the matrix when $\xi < 1$, which results in tensile

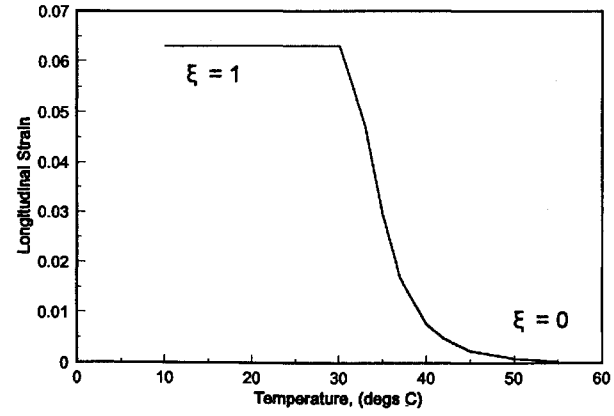

Fig. 5 Temperature-induced axial strain actuation with of 30% fiber volume ratio Ni-44.8wt% Ti/epoxy composite with reverse phase transformation in the fibers. Composite remains under stress-free conditions.

radial and longitudinal stresses in the fiber. These stresses alter the effective stress in the fiber [see Eqs. (23) and (24)], and to have continuous reduction in the martensite fraction, the mechanical stress on the composite should be adjusted. It is believed that such an adjustment is shown in Fig. 4, by the nonmonotonic stress variation during the reverse transformation. Apparently, the evolution of tensile radial stresses in the fiber reduces the effective stress beyond a point that makes it impossible to achieve certain ranges of martensite fractions, unless the applied mechanical stress on the composite is increased. In other words, Fig. 4 shows that to have continuous monotonic decrease in the martensite fraction of the fibers, the axial stress needs to increase and decrease again. This type of behavior is expected to be observed in a strain controlled uniaxial test.

The predicted capability of the composite to induce axial strain, under zero axial stress conditions, by controlling the temperature in the composite is shown in Fig. 5. The curve corresponds to a composite with stress-free austenite fibers. The curve begins at 20°C when the fibers are in the martensitic phase. The reverse transformation starts at 30°C and finishes at 55°C when the fibers have been fully transformed into austenite. It was predicted that a 25°C variation in temperature will result in a recovery strain of 6.3%.

Local Stresses

The predicted local stress distributions in the composite are presented here. The calculation of the stresses in the fiber and the matrix is important to ensure the integrity of the composite and prevent microcracking and fiber–matrix debonding. The longitudinal, radial, and hoop stresses are shown in Figs. 6–9 as functions of the normalized radius for various phases of the isothermal stress–strain cycle shown in Fig. 2. The normalized radius in the figures is defined as the ratio of the local radius to the radius of the fiber (r/r_f).

Figure 6 shows the stresses in the composite, when an average longitudinal stress $\sigma_{cx} = -53.6$ MPa is applied and the fibers still remain in the austenitic phase. Figure 7 shows the stresses in the composite when the fibers undergo martensitic transformation ($\xi = 0.83$) under the application of a tensile stress ($\sigma_{cx} = 176$ MPa). The applied tensile stress results in tensile longitudinal stresses in both the fiber and the matrix and in a tensile hoop stress in the matrix. Figure 8 shows the local stress in the composite during unloading with fully transformed fibers ($\xi = 1$ and $\sigma_{cx} = 288$ MPa). In spite of the significant increase in the average applied stress, there is little change in the magnitudes of the radial and hoop stresses, but the longitudinal stresses in the fibers and the matrix increase significantly. Figures 7 and 8 clearly show the significant contributions that the fiber transformation strains may have on the local stresses. The effect of these transformation-induced stresses on the composite response was discussed in the previous subsection.

Predicted stress distributions corresponding to the reverse phase transformation in the fibers ($\xi = 0.40$ and $\sigma_{cx} = 12$ MPa) are shown in Fig. 9. A comparison indicates that the stresses tend to return to a distribution similar to the one shown in Fig. 6. Further reduction of the longitudinal stress to -53.6 MPa resulted in full recovery of the parent phase in the fibers ($\xi = 0$) and yielded a stress distribution

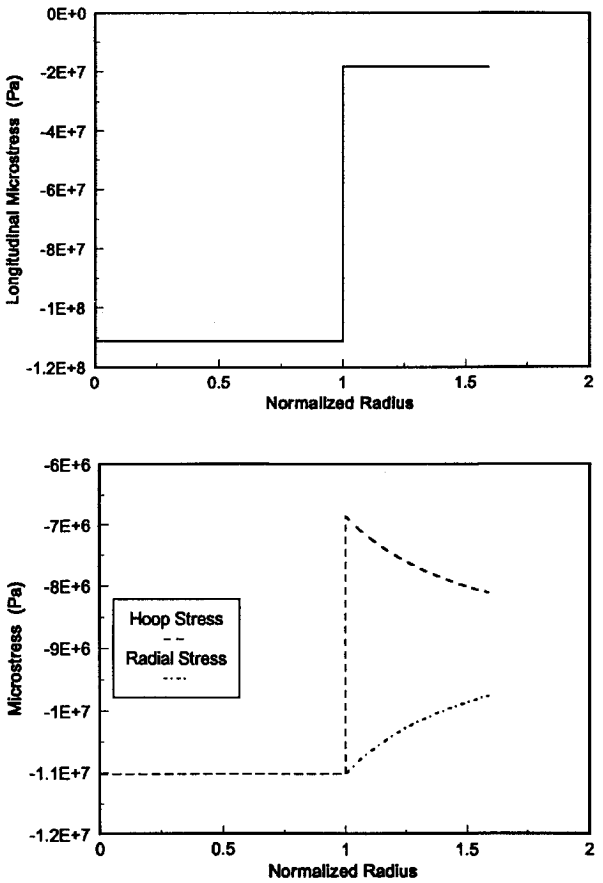

Fig. 6 Distribution of microstresses in Ni-44.8wt% Ti/epoxy composite with fibers in the parent (austenite) phase ($\sigma_{cx} = -53.6$ MPa and $\xi = 0$). Isothermal loading cycle at 40°C.

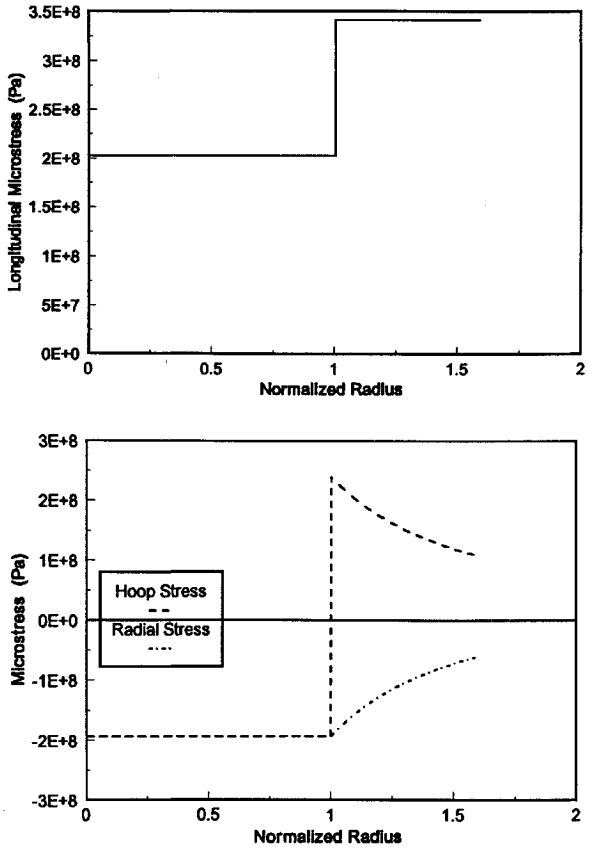

Fig. 8 Distribution of microstresses in Ni-44.8wt% Ti/epoxy composite with fibers fully transformed to the martensite phase ($\sigma_{cx} = 288$ MPa and $\xi = 1$). Isothermal loading cycle at 40°C.

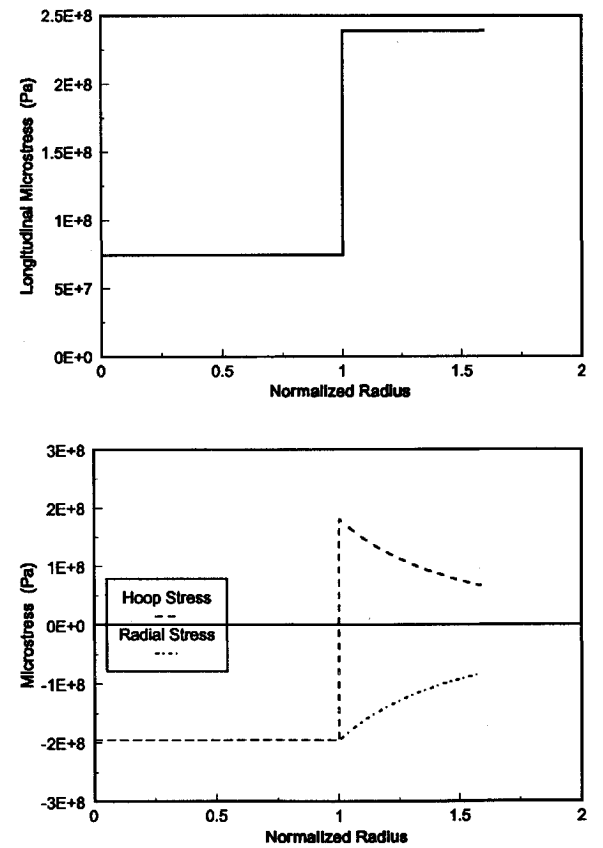

Fig. 7 Distribution of microstresses in Ni-44.8wt% Ti/epoxy composite with fibers undergoing martensite phase transformation ($\sigma_{cx} = 176$ MPa and $\xi = 0.83$). Isothermal loading cycle at 40°C.

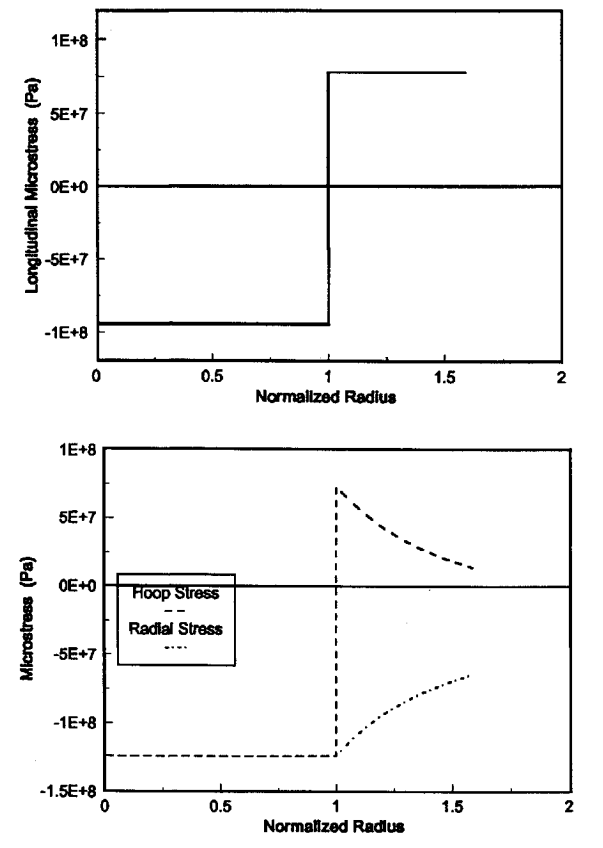

Fig. 9 Distribution of microstresses in Ni-44.8wt% Ti/epoxy composite with fibers undergoing reverse transformation ($\sigma_{cx} = 12$ MPa and $\xi = 0.40$). Isothermal loading cycle at 40°C.

identical to the one shown in Fig. 6. This is not surprising, because a reversible thermoelastic SM effect was assumed and at this point both loading and unloading curves coincide; hence, the corresponding internal stress states in the composite should be identical.

Summary

Micromechanics for the evaluation of the properties and analysis of stress in unidirectional composite systems with continuous SMA fibers in an elastic matrix were presented. The multicell micromechanical method was extended to calculate the average properties of the composite when the fibers undergo martensite or reverse phase transformations. The axial response of the composite and the local stresses in the fiber and the matrix were determined using a concentric cylinder model, where the fiber and the surrounding matrix are embedded within an infinite composite medium.

Applications of the mechanics were presented for a Ni-44.8wt% Ti/epoxy composite system. The numerical results demonstrated the longitudinal response of the composite under isothermal loading and unloading conditions. They also illustrated the capability of the composite to induce substantial longitudinal strains under variation of temperature. The ranges of stress, strain, and temperature where martensite and reverse phase transformations occur were also shown. It was predicted that substantial actuation strains may be induced in composites of intermediate fiber volume fraction ($\sim$0.3). It was also shown that the range of stress and strain where the composite may be used as actuator may be modified by controlling the stress-free conditions in the composite. Finally, the distribution of microstresses was considered for an entire isothermal loading-unloading cycle of the composite material with stress-induced phase transformation. The characteristic distribution of stresses remained unaffected, but their magnitude and sign changed drastically, depending on the martensite fraction of the fibers and the applied external load. In closing, this work represents an effort towards understanding and modeling the complex, yet promising, active response of continuous SMA fiber composites. Additional analytical and experimental work should be conducted in the future.

Appendix: Thermoelastic Properties

The elastic properties of SM composites using the multicell method[21–25] are

$$E_L = E_f k_f + E_m k_m \tag{A1}$$

$$E_T = E_m \left\{ 1 - \sqrt{k_f} + \frac{\sqrt{k_f}}{1 - \sqrt{k_f}[1 - (E_m/E_f)]} \right\} \tag{A2}$$

$$G_{LT} = G_M \left\{ 1 - \sqrt{k_f} + \frac{\sqrt{k_f}}{1 - \sqrt{k_f}[1 - (G_m/G_f)]} \right\} \tag{A3}$$

$$G_{TT} = \frac{G_m}{1 - \sqrt{k_f}[1 - (G_m/G_f)]} \tag{A4}$$

$$\nu_{LT} = \nu_f k_f + \nu_m k_m \tag{A5}$$

$$\nu_{TT} = (E_T/2G_{TT}) - 1 \tag{A6}$$

The coefficients of thermal expansion are

$$\alpha_L = \frac{E_f \alpha_f k_f + E_m \alpha_m k_m}{E_L} \tag{A7}$$

$$\alpha_T = \frac{E_m}{E_T} \left[\alpha_m (1 - \sqrt{k_f}) + \sqrt{k_f} \frac{\alpha_f \sqrt{k_f} + \alpha_m (1 - \sqrt{k_f})}{1 - \sqrt{k_f}[1 - (E_m/E_f)]} \right] \tag{A8}$$

where E_m, G_m, ν_m, and α_m are the normal and shear moduli of elasticity, the Poisson's ratio, and the coefficient of thermal expansion of the matrix, respectively; and ν_f is the Poisson's ratio of the fiber, which is independent of the martensite fraction. Volume fractions of the fiber and the matrix are denoted by k_f and k_m, respectively. Subscripts L and T identify the longitudinal and transverse directions.

Acknowledgment

This research was conducted during an American Society for Engineering Education summer (1994) faculty fellowship of Victor Birman at the NASA Lewis Research Center.

References

[1]Duerig, T. W., Melton, K. N., Stokel, D., and Wayman, C. M.,*Engineering Aspects of Shape Memory Alloys*, Butterworth–Heinemann, London, 1990.

[2]Schetky, L. M., and Wu, M. H., "The Properties and Processing of Shape Memory Alloys for Use as Actuators in Intelligent Composite Materials," *Smart Structures and Materials*, edited by G. K. Haritos and A. V. Srinivasan, American Society of Mechanical Engineers, New York, 1991, pp. 65–71.

[3]Schetky, L. McD., "The Role of Shape Memory Alloys in Smart/Adaptive Structures," *Shape-Memory Materials and Phenomena—Fundamental Aspects and Applications*, edited by C. T. Liu, H. Kunsmann, K. Otsuka, and M. Wutting, Vol. 246, Materials Research Society Symposium Proceedings, Materials Research Society, Pittsburgh, PA, 1992, pp. 299–307.

[4]White, S. R., Whitlock, M. E., Ditman, J. B., and Hebda, D. A., "Manufacturing of Adaptive Graphite/Epoxy Structures with Embedded Nitinol Fibers," *Adaptive Structures and Material Systems*, edited by G. P. Carman and E. Garcia, American Society of Mechanical Engineers, New York, 1993, pp. 71–79.

[5]Airoldi, G., Riva, G., Ranucci, T., and Vicentini, B., "Electric Transport Properties of a NiTi Shape Memory Alloy Under Applied Stress," *Shape-Memory Materials and Phenomena—Fundamental Aspects and Applications*, edited by C. T. Liu, H. Kunsmann, K. Otsuka, and M. Wutting, Vol. 246, Materials Research Society Symposium Proceedings, Materials Research Society, Pittsburgh, PA, 1992, pp. 277–281.

[6]Baumgart, F., Jorde, J., and Reiss, H. G., "Memory Alloys—Properties, Phenomenological Theory and Applications," NASA TM-77904; translation from German: Technische Mitteilunger Krupp, Forschungsberichte, Vol. 34, July 1976.

[7]Tanaka, K., "A Thermomechanical Sketch of Shape Memory Effect: One Dimensional Tensile Behavior," *Res Mechanica*, Vol. 18, 1986, pp. 251–263.

[8]Sato, Y., and Tanaka, K., "Estimation of Energy Dissipation in Alloys due to Stress-Induced Martensitic Transformation," *Res Mechanica*, Vol. 23, 1988, pp. 381–393.

[9]Brinson, L. C., "One-Dimensional Constitutive Behavior of Shape Memory Alloys: Thermomechanical Derivation with Non-Constant Material Functions and Redefined Martensite Internal Variable," *Journal of Intelligent Material Systems and Structures*, Vol. 4, April 1993, pp. 229–242.

[10]Liang, C., and Rogers, C. A., "One-Dimensional Thermomechanical Constitutive Relations for Shape Memory Materials," *Journal of Intelligent Material Systems and Structures*, Vol. 1, April 1990, pp. 207–234.

[11]Lin, M. W., and Rogers, C. A, "Analysis of Stress Distribution in a Shape Memory Alloy Composite Beam," AIAA Paper 91-1164, April 1991.

[12]Baz, A., Imam, K., and McCoy, J., "Active Vibration Control of Flexible Beams Using Shape Memory Actuators," *Journal of Sound and Vibration*, Vol. 140, Aug. 1990, pp. 437–456.

[13]Baz, A., and Chen, T., "Performance of Nitinol-Reinforced Drive Shafts," *Smart Structures and Intelligent Systems*, edited by N. W. Hagood and G. J. Knowles, Vol. 1917, Pt. 2, Society of Photo-Optical Instrumentation Engineers, Bellingham, WA, 1993, pp. 791–808.

[14]Brinson, L. C., and Lammering, R., "Finite Element Analysis of the Behavior of Shape Memory Alloys and Their Applications," *International Journal of Solids and Structures*, Vol. 30, No. 23, 1993, pp. 3261–3280.

[15]Liang, C., and Rogers, C. A., "The Multi-Dimensional Constitutive Relations of Shape Memory Alloys," AIAA Paper 91-1165, April 1991.

[16]Boyd, J. G., and Lagoudas, D. C., "Thermomechanical Response of Shape Memory Composites," *Smart Structures and Intelligent Systems*, edited by N. W. Hagood and G. J. Knowles, Vol. 1917, Pt. 2, Society of Photo-Optical Instrumentation Engineers, 1993, Bellingham, WA, pp. 774–790.

[17]Mori, T., and Tanaka, K., "Average Stress in Matrix and Average Elastic Energy of Materials with Misfitting Inclusions," *Acta Metallurgica*, Vol. 21, May 1973, pp. 571–574.

[18]Sullivan, B. J., and Buesking, K. W., "Structural Integrity of Intelligent Materials and Structures," Final Rept., U.S. Air Force Office of Scientific Research, AFOSR-TR 94 0388, Bolling AFB, Washington, DC, Feb. 1994.

[19]Hashin, Z., "Analysis of Properties of Fiber Composites with Anisotropic Constituents," *Journal of Applied Mechanics*, Vol. 46, No. 3, 1979, pp. 543–550.

[20]Noor, A. K., and Shah, R. S., "Effective Thermoelastic and Thermal Properties of Unidirectional Fiber-Reinforced Composites and Their Sensitivity Coefficients," *Composite Structures*, Vol. 26, No. 1–2, 1993, pp. 7–23.

[21]Chamis, C. C., "Simplified Composite Micromechanics Equations for Hygral, Thermal and Mechanical Properties," *SAMPE Quarterly*, Vol. 15, 1984, pp. 14–23; see also NASA TM 83320, 1983.

[22]Boyd, J. G., and Lagoudas, D. C., "A Thermodynamical Constitutive Model for Shape Memory Materials: Part 1. The Monolithic Shape Memory Alloy," *International Journal of Plasticity* (to be published).

[23]Wayman, C. M., and Duerig, T. W., "An Introduction to Martensite and Shape Memory," *Engineering Aspects of Shape Memory Alloys*, edited by T. W. Duerig, K. N. Melton, D. Stöckel, and C. M. Wayman, Butterworth–Heinemann, London, 1990, pp. 3–2019.

[24]Hopkins, D. A., and Chamis C. C., "A Unique Set of Micromechanics Equations for High Temperature Metal Matrix Composites," NASA TM-87154, 1985.

[25]Gibson, R. F., *Principles of Composite Material Mechanics*, McGraw–Hill, New York, 1994, pp. 77–83.

[26]Lei, C. Y., and Wu, M. H., "Thermomechanical Properties of NiTi-base Shape Memory Alloys," *Smart Structures and Materials*, edited by G. K. Haritos and A. V. Srinivasan, American Society of Mechanical Engineers, New York, 1991, pp. 73–77.